

Dissociative recombination and resonant ion-pair formation in electron collisions with HD^+

Johan Hörnquist^{1,*}, Ann E. Orel,² and Åsa Larson¹

¹*Department of Physics, Stockholm University, AlbaNova University Center, SE-106 91 Stockholm, Sweden*

²*Department of Chemical Engineering, University of California, Davis, California 95616, USA*



(Received 29 February 2024; accepted 23 April 2024; published 7 May 2024)

We have developed a method for which a variety of reactive scattering processes involving the H_2 reaction complex can be studied using the same set of potential curves and couplings. The method is based on a close-coupling approach in a strict diabatic representation. By rigorously incorporating nonadiabatic couplings among bound states, we enable the computation of final-state distributions. Loss into the ionization continuum is accounted for with a nonlocal complex potential matrix. The method has successfully been applied in studies of $\text{H}^+ + \text{H}^-$ mutual neutralization and $\text{H}(1s) + \text{H}(ns)$ associative ionization. In this paper, we investigate the applicability of this method to dissociative recombination and resonant ion-pair formation in electron collisions with HD^+ . The importance of a nonlocal description of autoionization is demonstrated. Calculated cross sections and final-state distributions are compared with results from experiments and previous theoretical studies.

DOI: [10.1103/PhysRevA.109.052806](https://doi.org/10.1103/PhysRevA.109.052806)

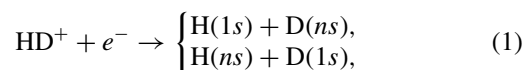
I. INTRODUCTION

Dissociative recombination (DR) is an elementary reactive scattering process in which an electron is captured by a molecular cation, resulting in dissociation into neutral fragments. The process is important in low-temperature plasmas, such as interstellar clouds, planetary atmospheres, and fusion plasma in the diverter region [1–5]. There are two competing mechanisms of DR. In the *direct mechanism*, the electron becomes temporarily trapped in a doubly excited dissociative metastable state which is then stabilized by dissociating into the neutral fragments. There is also the *indirect mechanism*, first proposed by Bardsley [6], in which the electron is captured in a rovibrationally excited Rydberg state which is then followed by predissociation by coupling to a state that is open for dissociation. Since there are multiple pathways in the potential landscape leading to dissociation, it may also be that the system dissociates into oppositely charged fragments, which is a process called resonant ion-pair formation (RIP).

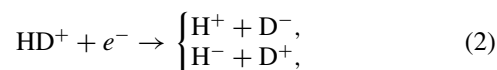
The simplest molecular ion for which DR may occur is H_2^+ , and this system has therefore been used as a benchmark system for comparison between experiment and theory. Early experiments on DR for this system were performed using single-pass merged beams [7–9]. The lack of control over the precise distribution of vibrational and rotational excitation of the ion beam made it hard to obtain a fair comparison between theory and experiment. By using ion-storage rings, many DR

experiments are carried out using HD^+ ions [10–15], allowing for radiative vibrational relaxation prior to the measurement due to the permanent dipole moment of the ion. While the ions in these room-temperature storage-ring experiments are known to be vibrationally relaxed, they are not rotationally relaxed, and including rotational effects in theoretical calculations has been found to be crucially important.

Theoretically, a variety of different methods such as time-dependent wave-packet methods [16,17], multichannel quantum defect theory (MQDT) [11,15,18–20], and configuration-interaction theory [6,21] have been applied to study DR of H_2^+ and its isotopologues. While the MQDT method has been proved to be successful in calculating the total DR cross section, it has been unable to provide branching ratios for the process. We have developed a method which relies on a close-coupling approach using *ab initio* calculated adiabatic potential curves and nonadiabatic couplings. Because of the inclusion of nonadiabatic couplings, we are able to follow the dynamics of the scattering process from small to large internuclear distances, allowing for the computation of not only the total DR cross section but also branching ratios to different products, including ionic fragments. We previously applied this method to study $\text{H}^+ + \text{H}^-$ mutual neutralization [22] and $\text{H}(1s) + \text{H}(ns)$ associative ionization [23]. In this paper, we apply this method for the DR process,



as well as the RIP process,



where the ion is in its ground vibrational state. The strength of this method is not that it is adjusted to obtain the most accurate cross section for a specific process, but rather that

*johan.hornquist@fysik.su.se

Published by the American Physical Society under the terms of the [Creative Commons Attribution 4.0 International](https://creativecommons.org/licenses/by/4.0/) license. Further distribution of this work must maintain attribution to the author(s) and the published article's title, journal citation, and DOI. Funded by [Bibsam](https://www.bibsam.org/).

it is a global method which is capable of treating a variety of different reactive scattering processes at the same level of theory. The aim of this paper is to investigate the applicability of the method to the DR and RIP processes.

In Sec. II we outline the main parts of the theoretical treatment. We discuss the potential curves, nonadiabatic couplings, and the transformation to a strict diabatic representation. The relevant equations governing the nuclear dynamics are also discussed. In Sec. III we present the results, including the total DR rate coefficient, branching ratios, and the RIP cross section. The results are compared with previous experimental and theoretical results.

Throughout the paper, atomic units are used unless otherwise specified.

II. THEORY

In this paper we use the model developed and described in our previous papers [22,23], and we will here give only a summary of the main parts. The reader is referred to those papers for more details.

A. Potential curves and couplings

In order to properly describe the nuclear dynamics and to calculate DR branching ratios, it is crucial to include nonadiabatic couplings among the states involved in the process. We previously calculated *ab initio* adiabatic potential curves as well as radial and rotational nonadiabatic couplings for excited states of H₂, including states up to the H(1s) + H(*n* = 4) asymptotic limit, for the symmetries ¹Σ_g⁺, ¹Σ_u⁺, ¹Π_g, and ¹Π_u. In addition, we also calculated the adiabatic potential curves and radial nonadiabatic couplings *ab initio* for the three lowest states of the ³Σ_u⁺ symmetry. To describe autoionization, the potentials and autoionization widths of the relevant electronic resonant states also need to be computed. We previously computed these data for the lowest-lying resonant states of the above symmetries, including the ³Σ_g⁺ symmetry, by performing electron-scattering calculations on H₂⁺. For nuclear geometries where the resonant state potential has crossed the ion potential, we use an optimization procedure (based on quasidiabatic potentials as described below). More details can be found in [22]. In the present paper, we focus on DR for low collision energies (<2.5 eV). In this energy region, it is well established that the lowest resonant state of the ¹Σ_g⁺ symmetry contributes the most to DR. We will therefore assume in our calculations that this is the only symmetry contributing to the low-energy DR cross section. It has been found (see, e.g., Ref. [20]) that, within the MQDT framework, including symmetries that are rotationally compatible with ¹Σ_g⁺ can significantly alter the DR cross section at low collision energies. It must be pointed out, however, that in our framework, these symmetries are coupled via rotational nonadiabatic couplings and that these couplings are not included in Ref. [20]. We will investigate the effect of rotational nonadiabatic couplings on the low-energy DR cross section by including these couplings between states of the ¹Σ_g⁺ and ¹Π_g symmetries. For the RIP process, it is essential to include contributions from the ¹Σ_u⁺ symmetry at high collision energies [24]. Therefore, we consider both the ¹Σ_g⁺ and ¹Σ_u⁺ symmetries for that process.

In order to include autoionization, a quasidiabatic model is introduced at small internuclear distances. In this model, we include the lowest resonant state of a given symmetry and an arbitrary number of Rydberg states. The Rydberg state potentials are given by the formula

$$V_i(R) = V_{\text{ion}}(R) - \frac{1}{2[n_i - \mu_l^d(R)]^2}, \quad (3)$$

where $\mu_l^d(R)$ is the diabatic quantum defect, n_i is the principal quantum number, and l is the orbital angular momentum quantum number of the Rydberg electron. We assume in this model that there are no couplings between the Rydberg states but that the Rydberg states couple to the resonant state via [25]

$$V_{ri}(R) = \sqrt{\frac{\Gamma_l(R)}{2\pi}} [n_i - \mu_l^d(R)]^{-3/2}, \quad (4)$$

where $\Gamma_l(R)$ is the partial autoionization width. In the present paper, we include the *s* and *d* partial autoionization widths for the resonant states of the ¹Σ_g⁺ symmetry as well as the *p* and *f* partial autoionization widths for the ¹Σ_u⁺ symmetry. The total autoionization width is the sum of the partial autoionization widths, i.e., $\Gamma(R) = \sum_l \Gamma_l(R)$. The quasidiabatic potentials are then diagonalized. The resulting adiabatic potentials, given as a transformation $\mathbf{V}^{ad} = \mathbf{S}^T \mathbf{V}^{qd} \mathbf{S}$, approximate the Born-Oppenheimer potentials at small internuclear distances. The transformation matrix \mathbf{S} is also used to obtain approximate radial nonadiabatic couplings. The approximate adiabatic potentials and nonadiabatic couplings are then combined with the *ab initio* calculated adiabatic potentials and nonadiabatic couplings. Thus, for the lower electronic states, *ab initio* calculated potentials and nonadiabatic couplings are used, while for higher-lying states, potentials and nonadiabatic couplings extracted from the quasidiabatic potential matrix are incorporated. This yields a set of adiabatic potentials and nonadiabatic couplings that can be used to describe both autoionization at small internuclear distances and nonadiabatic interactions at various internuclear distances. In Fig. 1, the adiabatic potentials in ¹Σ_g⁺ symmetry are displayed.

In the next step, a strict diabatic representation is obtained by the transformation $\mathbf{V}^d = \mathbf{T}^T \mathbf{V}^{ad} \mathbf{T}$, where the orthogonal adiabatic-to-diabatic transformation matrix \mathbf{T} is a solution of the equation [26]

$$\left(\mathbf{I} \frac{d}{dR} + \boldsymbol{\tau}(R) \right) \mathbf{T}(R) = \mathbf{0}, \quad (5)$$

where \mathbf{I} is the identity matrix and $\boldsymbol{\tau}$ is a matrix consisting of the first derivative nonadiabatic couplings.

B. Nuclear equations

We use a close-coupling approach to study DR and RIP. The cross section is calculated by solving the coupled Schrödinger equation in a strict diabatic representation,

$$\frac{d^2}{dR^2} \boldsymbol{\Psi}^J(R) + \mathbf{f}^J(R) \boldsymbol{\Psi}^J(R) = \int dR' \mathbf{g}(R, R') \boldsymbol{\Psi}^J(R'), \quad (6)$$

where J is the angular momentum quantum number of the formed molecular complex and $\boldsymbol{\Psi}$ is the wave-function matrix.

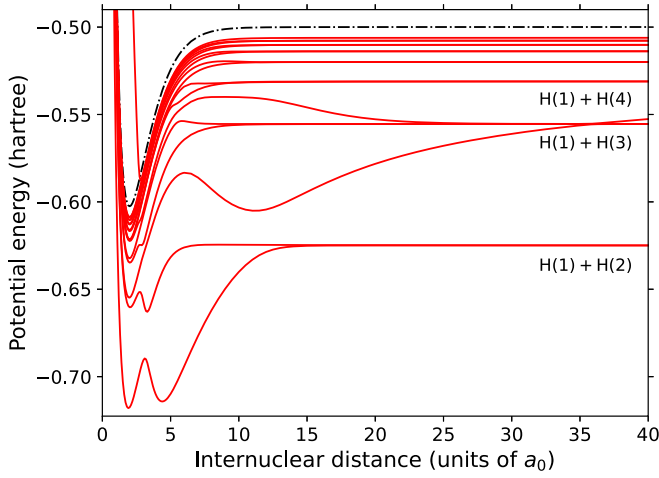


FIG. 1. Adiabatic potential-energy curves of H_2 in $^1\Sigma_g^+$ symmetry. The ground-state potential is not shown. The black dash-dotted curve is the potential of H_2^+ . The asymptotic limits corresponding to $n = 2, 3, 4$ are indicated on the right.

The elements of \mathbf{f}^J are given by

$$f_{ij}^J(R) = 2\mu \left[E\delta_{ij} - \frac{J(J+1)}{2\mu R^2}\delta_{ij} - V_{ij}^d(R) \right], \quad (7)$$

where μ is the reduced mass of the system. The right-hand side of Eq. (6) is a nonlocal complex potential. Here, we do not consider the real part of this potential, which represents a level shift. The imaginary part of the complex potential describes loss due to autoionization and can be expressed as [25,27]

$$\begin{aligned} g_{ij}(R, R') = & -i\mu \sum_{mnvJ'l} (2J' + 1) \begin{pmatrix} J & J' & l \\ \Lambda & 0 & -\Lambda \end{pmatrix}^2 \\ & \times T_{im}^T(R) S_{mr}^T(R) \sqrt{\Gamma_l(R)} \chi_v^J(R) \\ & \times \chi_v^{J'}(R') \sqrt{\Gamma_l(R')} S_{rn}(R') T_{nj}(R'). \end{aligned} \quad (8)$$

The sum over m and n runs over the diabatic states included in the model, that over v runs over the vibrational channels of the ion that are open at a given collision energy, that over l runs over the angular momentum quantum number of the free electron, and that over J' runs over the angular momentum of the molecular ion. $S_{ij}(R)$ are elements of the quasidiabatic-to-adiabatic transformation matrix, which is defined above. The subscript r refers to the resonant state, and Λ is the projection of the electronic orbital angular momentum quantum number on the internuclear axis. If rotational couplings are not considered, Eq. (6) is solved separately for each symmetry considered. When rotational couplings are included, Eq. (6) is slightly modified (see Ref. [22]) and has to be solved simultaneously for the symmetries that are rotationally coupled.

A common approximation is the local approximation [28–31], in which it is assumed that the open vibrational channels form a complete set at any energy. This yields

$$\frac{d^2}{dR^2} \Psi^J(R) + \mathbf{f}^J(R) \Psi^J(R) = \mathbf{W}(R) \Psi^J(R). \quad (9)$$

In this expression, the matrix $\mathbf{W}(R)$ is a local complex potential given by

$$W_{ij}(R) = -i\mu \sum_{mn} T_{im}^T(R) S_{mr}^T(R) \Gamma(R) S_{rn}(R) T_{nj}(R), \quad (10)$$

where $\Gamma(R)$ is the total autoionization width. For DR at low collision energies, the local approximation is not expected to be valid because it overestimates the autoionization [16]. By performing calculations with both the local and nonlocal complex potentials, the local approximation can be tested.

The integro-differential Eq. (6) is solved, as described in [23], by using the solution of Eq. (9) as a first guess in the nonlocal term on the right-hand side and then iterating until convergence. An iteration is considered to be converged when the relative difference between two successive partial cross sections is less than 10^{-5} . The average number of iterations needed to reach convergence was of the order of 10 iterations in all calculations. The wave-function matrix is determined by matching the numerical solution at sufficiently large internuclear distances with the appropriate boundary conditions, which are set up such that each column in the wave-function matrix asymptotically represents dissociation into a specific final state.

C. Cross section

From the nuclear wave-function matrix, $\Psi^J(R)$, the cross section for electron capture of the molecular ion in an initial rovibrational state (v, J') and dissociating into a final state i is obtained from the expression [32]

$$\begin{aligned} \sigma(E, E_v^{J'}) = & g \frac{4\pi^3}{k_i^2} \sum_{Jl} (2J+1) \begin{pmatrix} J & J' & l \\ \Lambda & 0 & -\Lambda \end{pmatrix}^2 \\ & \times \left| \sum_{mn} \langle \chi_v^{J'} | T_{mn}(R) S_{rm}(R) \sqrt{\frac{\Gamma_l(R)}{2\pi}} | \psi_{ni}^J \rangle \right|^2. \end{aligned} \quad (11)$$

The total DR cross section is obtained by summing over all final states i , while the branching ratios are obtained by summing over the final states associated with a specific limit and then dividing by the total DR cross section. The RIP cross section is obtained by choosing the ion-pair states of the $^1\Sigma_g^+$ or $^1\Sigma_u^+$ symmetry as the final state. The factor g is the statistical weight, and it is given by the multiplicity of the final state divided by the multiplicity of the initial state.

While the initial vibrational state of radiative active molecular ions such as HD^+ can be controlled in the room-temperature storage-ring experiments, the initial rotational state cannot, and the rotational distribution in such experiments is, in general, not well characterized. We will assume that the rotational population can be approximated by a Boltzmann distribution at a temperature of 300 K, which should be valid for comparison with the measurement of DR of HD^+ using The Heavy Ion Test Storage Ring [15]. Furthermore, in order to compare the theoretical cross section to experimental cross sections, the cross section needs to be convoluted with the experimental electron velocity distribution $f(\vec{v}_e)$. The rate coefficient is thus

given by

$$\alpha(v_d) = \int \sigma(v) v f(\vec{v}_e) d^3 v_e, \quad (12)$$

where v_d is the detuning velocity and $v = \sqrt{v_{e\perp}^2 + (v_d + v_{e\parallel})^2}$. Using an anisotropic Maxwellian distribution for $f(\vec{v}_e)$, the rate coefficient can be expressed as [33]

$$\alpha(E) = \int d\varepsilon \frac{\sigma(\varepsilon)}{kT_{e\perp} \lambda \sqrt{2m_e}} \sqrt{\frac{\varepsilon}{2m_e}} \exp\left(-\frac{\varepsilon - \frac{E}{\lambda^2}}{kT_{e\perp}}\right) \times \left[\operatorname{erf}\left(\frac{\lambda^2 \sqrt{\varepsilon} - \sqrt{E}}{\lambda \sqrt{kT_{e\parallel}}}\right) + \operatorname{erf}\left(\frac{\lambda^2 \sqrt{\varepsilon} + \sqrt{E}}{\lambda \sqrt{kT_{e\parallel}}}\right) \right], \quad (13)$$

where $\lambda = \sqrt{1 - \frac{T_{e\parallel}}{T_{e\perp}}}$. Here, $T_{e\perp}$ and $T_{e\parallel}$ are the experimental transverse and longitudinal electron temperatures, respectively.

III. RESULTS AND DISCUSSION

A. Convergence

With the quasidiabatic model it is possible to include an arbitrary number of Rydberg states. These states are added explicitly to the potential matrix used when solving the coupled Schrödinger equation, thus increasing the number of coupled equations that need to be solved iteratively. Convergence of the cross section (or rate coefficient) with respect to the number of states included therefore needs to be checked. To do this, we performed calculations of the total DR cross section, in which we successively add more Rydberg states to the calculation. These calculations were performed in the $^1\Sigma_g^+$ symmetry using the local approximation, which should be sufficient to check the convergence of the cross section with respect to the number of states included. In Fig. 2, we show the results, which are labeled according to the principal quantum number n representing the asymptotic limit $\text{H}(1s) + \text{D}(n)$. All cross sections were averaged over the rotational states $J' = 0-7$ using a Boltzmann distribution at 300 K. The resonances seen in the cross sections are due to temporary capture into bound rovibrational Rydberg states of the collision complex, i.e., states that are closed for dissociation at a given energy. Resonances originating from calculations with different J' are superimposed when the Boltzmann average is performed. The calculation including states up to the $n = 4$ asymptotic limit includes only the *ab initio* calculated potentials and it has fewer resonant structures because fewer closed states are included. As more states are added to the calculation, the number of resonances increases, and the cross section converges. The $n = 10$ calculation includes 21 states in total. When the number of states is increased to 29 ($n = 14$), only minor differences can be seen in the cross section. We therefore consider the DR cross section to be converged for $n = 10$, and hence, the remaining results in this study were therefore calculated including states up to the $n = 10$ asymptotic limit.

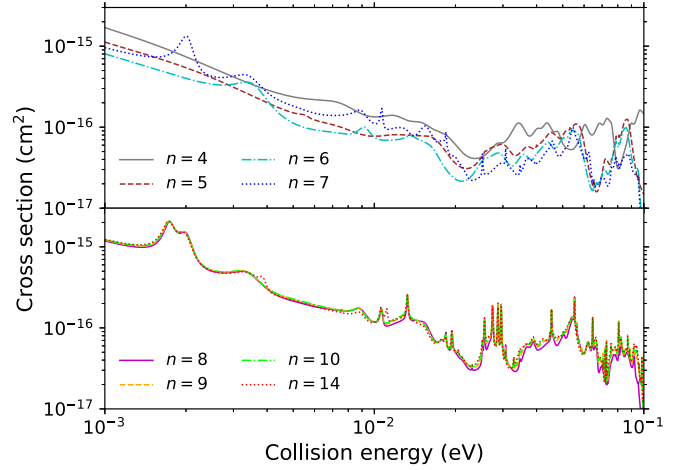


FIG. 2. Convergence of the DR cross section with respect to the number of states included. The calculations are labeled by the principal quantum number n , representing the asymptotic limit $\text{H}(1s) + \text{D}(n)$. Calculations including states up to the $n = 4-7$ limits are shown in the top panel, while calculations with $n = 8-14$ are shown in the bottom panel.

B. Total DR rate coefficient

The total DR rate coefficient for collisions between electrons and HD^+ ions in the ground vibrational state was calculated in the $^1\Sigma_g^+$ symmetry for initial ionic rotational quantum numbers of $J' = 0-7$ using a nonlocal complex potential. The rate coefficients for the different initial rotational quantum numbers were summed over a Boltzmann distribution at $T = 300$ K. The result, which was convoluted using function (13) with $kT_{e\perp} = 0.6$ meV and $kT_{e\parallel} = 0.025$ meV, is shown in Fig. 3 in comparison with previous experiment [15] and theory [19,20,34]. Resonances from the cross sections corresponding to different initial rotational states of the ion are superimposed when performing the Boltzmann average and are then smoothed when the cross section is convoluted. This is the origin of the structure seen in the rate coefficient. The present calculation reproduces the magnitude

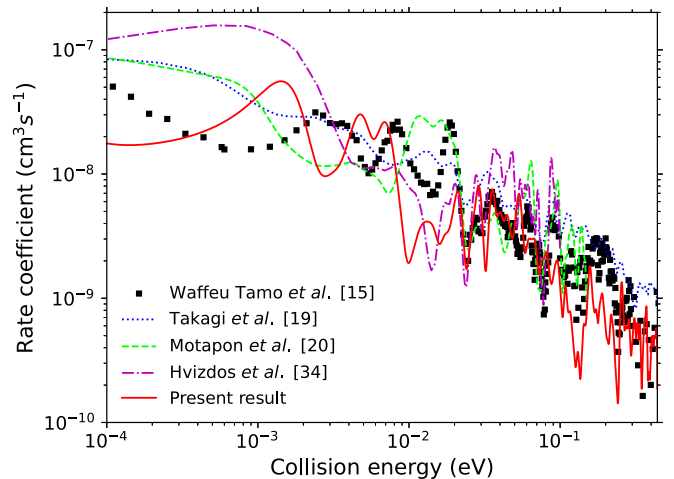


FIG. 3. The total DR rate coefficient in comparison with previous experiment [15] and theory [19,20,34].

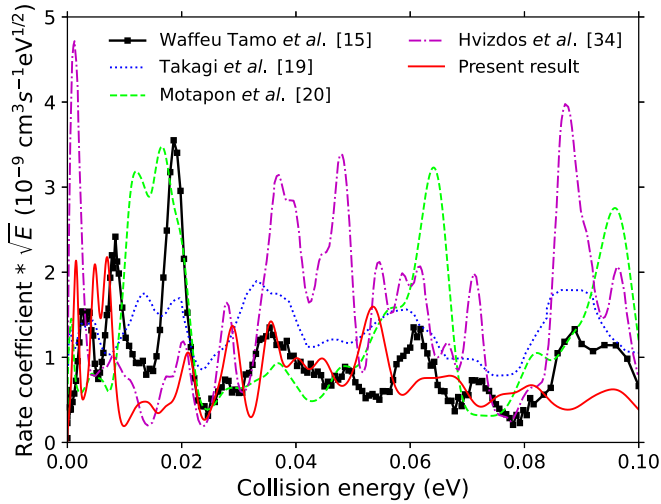


FIG. 4. Total DR rate coefficient multiplied by the square root of the energy, compared with previous experiment [15] and theory [19,20,34].

of the measured rate coefficient, but several of the structures do not coincide. At very low energies (< 1 meV), the present result is significantly lower than previous theoretical studies. In the present model, we do not include the indirect capture directly in the Rydberg states through nonadiabatic interactions. Since the potential of the lowest electronic resonant state of the $^1\Sigma_g^+$ symmetry, which is important for low-energy DR, crosses the ion potential close to the outer turning point of the ground rovibrational state of the ion, the indirect capture could be significant at very low energies. The present model does not include nonadiabatic coupling among the quasidiabatic Rydberg states or the nonadiabatic couplings between the Rydberg states and the ionization continuum. We believe this explains the lack of dense resonances observed in the MQDT calculations [15,20], in which these interactions are taken into account through the R dependence of the quantum defects. As the collision energy increases, the direct mechanism is likely to dominate, and the present calculation should therefore become more accurate as the energy increases. In the present model, it is possible to include the nonadiabatic couplings corresponding to indirect capture, which could be a subject for future development. A more detailed comparison between theory and experiment is shown in Fig. 4, where we show the total DR rate coefficient for collision energies below 0.1 eV multiplied by the square root of the collision energy to better resolve the structures.

In Fig. 5, we compare the DR rate coefficient calculated using a nonlocal complex potential to the rate coefficient calculated using the local approximation. At low collision energies, the calculation with the local approximation is about an order of magnitude smaller than the calculation using a nonlocal complex potential. Moreover, more structure can be seen in the nonlocal calculation, which better represents the structure seen in the measured cross section. As expected, the local approximation cannot accurately represent the loss in the ionization continuum at low collision energies since only one or a few vibrational channels are open. As the energy increases and more vibrational states become energetically

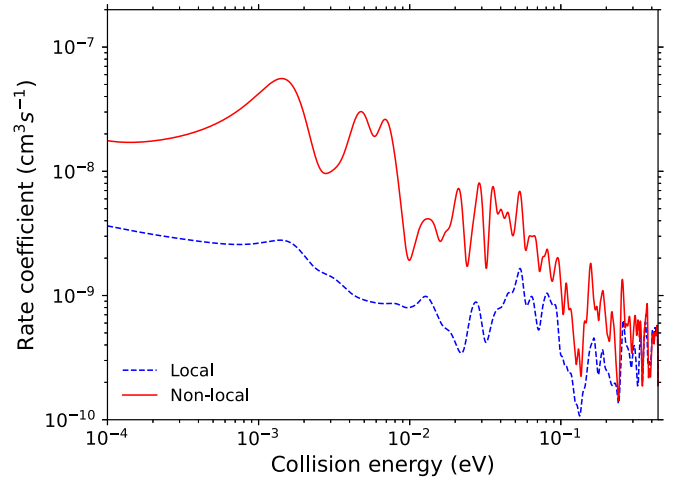


FIG. 5. Comparison of the total DR rate coefficient calculated with and without the local approximation.

open, the nonlocal complex potential converges to the local complex potential. As a result, the two calculations converge at higher collision energies, which is indicated in Fig. 5.

We also performed a calculation of the total DR rate coefficient including *ab initio* calculated rotational nonadiabatic couplings between bound states of the $^1\Sigma_g^+$ and $^1\Pi_g$ symmetries. The rotational nonadiabatic couplings are found to have a negligible effect on the total DR rate coefficient at low energies. This can be explained by the fact that at low collision energies, the direct contribution from capture in the lowest $^1\Pi_g$ resonant state is orders of magnitude smaller than the contribution from capture in the lowest $^1\Sigma_g^+$ resonant state.

C. Branching ratios

In addition to the total DR cross section, we also calculated the cross sections to specific final states. The branching ratios for final states of $n = 2$, $n = 3$, and $n = 4$ are shown in Fig. 6 in comparison with the experimental branching ratios of Ref. [35]. The present results are in reasonable agreement with experiment, especially for the $n = 2$ branching ratio. For energies above 1.8 eV, where the $n = 4$ channels open up for dissociation, we obtain a branching ratio to $n = 4$ that is slightly lower than the experiment. As a result, we obtain a slightly larger $n = 3$ branching ratio. It should be noted, as mentioned in our earlier work [22,23], that we were not able to obtain accurate adiabatic potential curves for all the $n = 4$ states of the $^1\Sigma_g^+$ symmetry. The fact that we lack some of the $n = 4$ states in our calculation could explain why we obtain a branching ratio to $n = 4$ that is smaller than the experimental one. By summing the $n = 3$ and $n = 4$ branching ratios and comparing to the equivalent experimental data, the present calculation agrees with the measured data also for the high collision energies.

D. RIP cross section

We calculated the RIP cross section in collisions of electrons with HD^+ , and the result is shown in Fig. 7 in comparison to the measurement in Ref. [36]. In the experiment, the $\text{H}^+ + \text{D}^-$ cross section was measured. It has since been

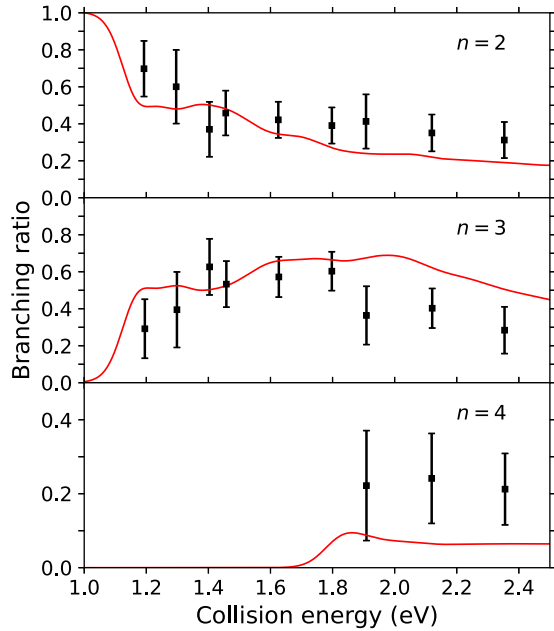


FIG. 6. Calculated DR branching ratios (solid curves) in comparison to the measured branching ratios of Ref. [35] (black squares).

established that the $D^+ + H^-$ RIP cross section has the same shape and magnitude as those of $H^+ + D^-$ [37]. With the present model, these two channels cannot be distinguished. As a result we can calculate only the total RIP cross section, and this cross section is divided by a factor of 2 for comparison with the experimental data.

The RIP cross section displays many oscillations. It was suggested by Ref. [36] and later confirmed by Refs. [17,24] that these oscillations arise due to quantum interference between different competing pathways leading to ion-pair formation. The present model includes nonadiabatic couplings between various bound states of the collision complex, ranging from small to large internuclear distances, and as such, it should be able to reproduce the oscillations in the cross

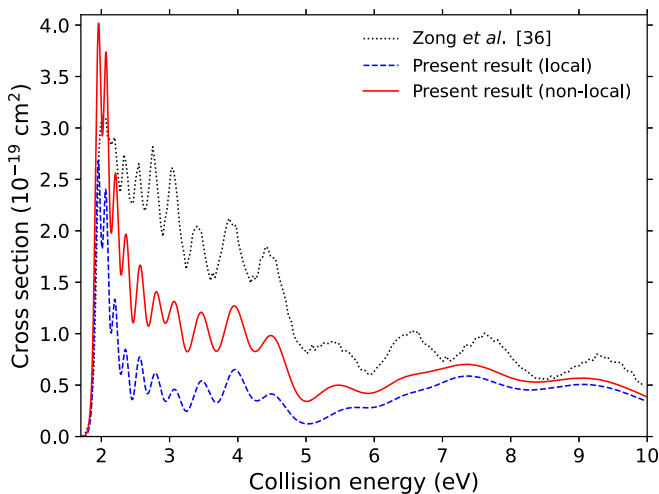


FIG. 7. Calculated RIP cross sections in comparison with the measured cross section of Ref. [36].

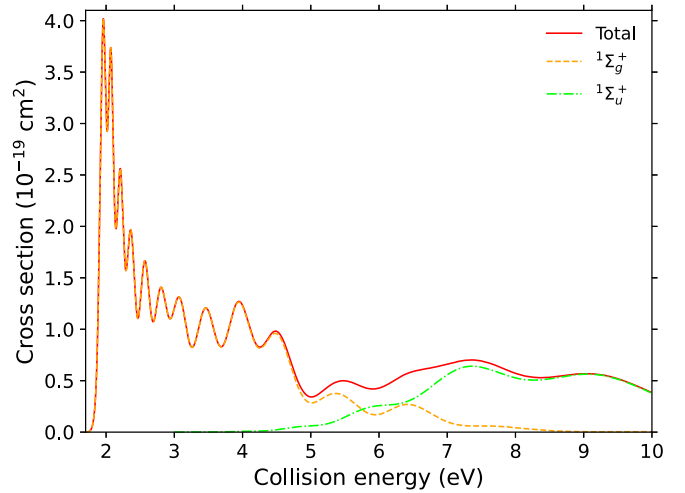


FIG. 8. The total RIP cross section (solid curve) in comparison with the contributions from states with $^1\Sigma_g^+$ (dashed curve) and $^1\Sigma_u^+$ (dash-dotted curve) symmetries.

section. Except for an extra peak at the threshold, the present calculation reproduces not only the number of peaks but also the period of the oscillations. This demonstrates the accuracy of the nonadiabatic couplings included in the calculation. The present calculation is about a factor of 2 smaller than the measured cross section at 2.3 eV, and the difference decreases as the collision energy increases. Also shown in Fig. 7 is the cross section calculated using the local approximation. The result suggests that a nonlocal description of autoionization is important to describe the loss in the ionization continuum for the RIP process, even at high collision energies. This was not considered in previous theoretical studies [17,24].

At collision energies of about 4.5 eV, the measured RIP cross section drops in magnitude and increases slightly again around 6 eV. This behavior is also seen in the present calculation. The increase of the cross section after 6 eV corresponds to the energies where the states of the $^1\Sigma_u^+$ symmetry become important, as shown in Fig. 8. At high collision energies, therefore, it is essential to include the contribution from the $^1\Sigma_u^+$ symmetry. While the oscillations seen in the experimental cross section are well reproduced by the calculation below 6 eV, they are less so at higher energies where the $^1\Sigma_u^+$ symmetry is dominant. At these energies, it is possible that higher-lying resonant states of the $^1\Sigma_u^+$ symmetry could start to contribute, which could also influence the oscillations in the cross section.

IV. SUMMARY

We developed a model of the H_2 reaction complex that can be used to compute cross sections of a variety of reactive scattering processes, such as mutual neutralization, associative ionization, double charge transfer, DR, and RIP, using the same set of potential curves and couplings. Here, we applied this model in calculations of the total DR rate coefficient and branching ratios as well as the RIP cross section for electron collisions with HD^+ . It was shown that a nonlocal description of autoionization is important for low-energy DR, as well as for the RIP process. While the magnitude of the total DR rate

coefficient is in agreement with experiment, the present calculation failed to reproduce the low-energy detailed structures of the measured rate coefficient. A possible explanation is that the present model does not include the indirect capture, which could be important at low collision energies. Furthermore, we have not considered the real part of the nonlocal complex potential in the present model. If this term is important, it could explain some of the discrepancy between the calculated and measured rate coefficients. Investigating the importance of this term for the DR process is beyond the scope of this paper but could be a subject for future development. Calculated DR branching ratios, as well as the cross section for ion-pair

formation, are in satisfactory agreement with the measured ones. The model accurately captures the quantum interference between competing pathways leading to dissociation into the ion-pair since both the magnitude and period of the structures in the RIP cross section agree well with the measurement.

ACKNOWLEDGMENTS

This work was performed as part of the project “Probing charge- and mass-transfer reactions on the atomic level,” supported by the Knut and Alice Wallenberg Foundation (Grant No. 2018.0028).

-
- [1] J. N. Bardsley and M. A. Biondi, *Adv. Mol. Phys.* **6**, 1 (1970).
[2] S. L. Guberman and A. Giusti-Suzor, *J. Chem. Phys.* **95**, 2602 (1991).
[3] J. L. Fox, *J. Geophys. Res.* **98**, 3297 (1993).
[4] W. D. Geppert and M. Larsson, *Chem. Rev.* **113**, 8872 (2013).
[5] A. Y. Pigarov, *Phys. Scr.* **T96**, 16 (2002).
[6] J. N. Bardsley, *J. Phys. B* **1**, 349 (1968).
[7] B. Peart and K. T. Dolder, *J. Phys. B* **7**, 236 (1974).
[8] D. Auerbach, R. Cacak, R. Caudano, T. D. Gaily, C. J. Keyser, J. W. McGowan, J. B. A. Mitchell, and S. F. J. Wilk, *J. Phys. B* **10**, 3797 (1977).
[9] H. Hus, F. Yousif, C. Noren, A. Sen, and J. B. A. Mitchell, *Phys. Rev. Lett.* **60**, 1006 (1988).
[10] P. Forck, M. Grieser, D. Habs, A. Lampert, R. Repnow, D. Schwalm, A. Wolf, and D. Zajfman, *Nucl. Instrum. Methods Phys. Res., Sect. B* **79**, 273 (1993).
[11] T. Tanabe *et al.*, *Phys. Rev. Lett.* **75**, 1066 (1995).
[12] C. Strömholm, I. F. Schneider, G. Sundström, L. Carata, H. Danared, S. Datz, O. Dulieu, A. Källberg, M. af Ugglas, X. Urbain, V. Zengin, A. Suzor-Weiner, and M. Larsson, *Phys. Rev. A* **52**, R4320(R) (1995).
[13] L. H. Andersen, P. J. Johnson, D. Kella, H. B. Pedersen, and L. Vejby-Christensen, *Phys. Rev. A* **55**, 2799 (1997).
[14] A. Al-Khalili *et al.*, *Phys. Rev. A* **68**, 042702 (2003).
[15] F. O. Waffeu Tamo *et al.*, *Phys. Rev. A* **84**, 022710 (2011).
[16] A. E. Orel, *Phys. Rev. A* **62**, 020701(R) (2000).
[17] Å. Larson and A. E. Orel, *Phys. Rev. A* **64**, 062701 (2001).
[18] I. F. Schneider, C. Strömholm, L. Carata, X. Urbain, M. Larsson, and A. Suzor-Weiner, *J. Phys. B* **30**, 2687 (1997).
[19] H. Takagi, S. Hara, and H. Sato, *Phys. Rev. A* **79**, 012715 (2009).
[20] O. Motapon, N. Pop, F. Argoubi, J. Zs Mezei, M. D. Epee Epee, A. Faure, M. Telmini, J. Tennyson, and I. F. Schneider, *Phys. Rev. A* **90**, 012706 (2014).
[21] A. P. Hickman, *J. Phys. B* **20**, 2091 (1987).
[22] J. Hörnquist, P. Hedvall, Å. Larson, and A. E. Orel, *Phys. Rev. A* **106**, 062821 (2022).
[23] J. Hörnquist, P. Hedvall, A. E. Orel, and Å. Larson, *Phys. Rev. A* **108**, 052811 (2023).
[24] Å. Larson *et al.*, *Phys. Rev. A* **62**, 042707 (2000).
[25] J. Weiner, F. Masnou-Seeuws, and A. Giusti-Suzor, *Adv. At., Mol., Opt. Phys.* **26**, 209 (1990).
[26] C. A. Mead and D. G. Truhlar, *J. Chem. Phys.* **77**, 6090 (1982).
[27] R. J. Bieniek, *J. Phys. B* **13**, 4405 (1980).
[28] A. Herzenberg, *J. Phys. B* **1**, 548 (1968).
[29] D. T. Birtwistle and A. Herzenberg, *J. Phys. B* **4**, 53 (1971).
[30] L. Dube and A. Herzenberg, *Phys. Rev. A* **11**, 1314 (1975).
[31] L. Dube and A. Herzenberg, *Phys. Rev. A* **20**, 194 (1979).
[32] R. J. Bieniek, *Phys. Rev. A* **18**, 392 (1978).
[33] H. Danared, *Phys. Scr.* **T59**, 121 (1995).
[34] D. Hvizdos, R. Curik, and C. H. Greene, *Eur. Phys. J. D* **76**, 45 (2022).
[35] D. Zajfman, Z. Amitay, M. Lange, U. Hechtischer, L. Knoll, D. Schwalm, R. Wester, A. Wolf, and X. Urbain, *Phys. Rev. Lett.* **79**, 1829 (1997).
[36] W. Zong *et al.*, *Phys. Rev. Lett.* **83**, 951 (1999).
[37] A. Neau, A. Derkatch, F. Hellberg, S. Rosén, R. Thomas, M. Larsson, N. Djuric, D. B. Popovic, G. H. Dunn, and J. Semaniak, *Phys. Rev. A* **65**, 044701 (2002).